

Dendritic asymmetry cannot account for directional responses of neurons in visual cortex

J. C. Anderson¹, T. Binzegger¹, O. Kahana², K. A. C. Martin¹ and I. Segev²

¹ Institute of Neuroinformatics, University/ETHZ, Winterthurerstr.190, 8057 Zurich, Switzerland

² Institute of Life Science and Center of Neural Computation, Hebrew University, Jerusalem, Israel

Correspondence should be addressed to K.A.C.M. (kevan@ini.phys.ethz.ch)

A simple model was proposed to account for the direction selectivity of neurons in the primary visual cortex, area V1. In this model, the temporal asymmetries in the summation of inhibition and excitation that produce directionality were generated by structural asymmetries in the tangential organization of the basal dendritic tree of cortical neurons. We reconstructed dendritic trees of neurons with known direction preferences and found no correlation between the small biases of a neuron's dendritic morphology and its direction preference. Detailed simulations indicated that even when the electrotonic asymmetries in the dendrites were extreme, as in cortical Meynert cells, the biophysical properties of single neurons could contribute only partially to the directionality of cortical neurons.

Several models have been proposed to account for direction selectivity of neurons. One correlation model for motion detection in the fly¹ uses temporal summation or multiplication of excitatory inputs in the preferred direction of motion. A model for the rabbit retina² uses inhibition of excitation in the non-preferred direction of motion to achieve directionality. Both of these mechanisms require a spatiotemporal asymmetry in the inputs for the two directions of motion. Livingstone³ proposed an interesting variant of this for neurons in the visual cortex. In her model, also reminiscent of earlier simulations⁴, excitatory synapses are activated sequentially along asymmetric basal dendrites of the large solitary pyramidal cells of Meynert. In response to the preferred direction, the synapses are activated sequentially from the dendrite tip to the soma. Here the dendrite acts as a delay line⁵, allowing the excitatory postsynaptic potentials (EPSPs) to summate temporally along the dendrite before inhibition is activated at the soma. When the synapses are activated sequentially from the soma to the dendritic tip, temporal summation is less effective and inhibition, now activated earlier, is more effective in reducing EPSP amplitude. It should be noted, however, that if excitation and inhibition sum linearly, then the areas under the voltage waveform would be equal for both directions, although the voltage waveform recorded in the soma will have a higher peak for the preferred direction. Thus, the essential nonlinearity required for directionality comes from the voltage threshold for spike firing.

The reason for choosing the solitary pyramidal cells first described by Meynert in 1872 is that the marked asymmetries in their basal dendrites^{6–9} would allow them to sample differentially from sectors of the two-dimensional retinotopic representation of visual space on the surface of V1. However, whereas Meynert cells are sparse (only 30×10^3 – 40×10^3 per hemisphere in the monkey, ~25 cells beneath each mm^2 of cortical surface¹⁰ and confined to one narrow sublayer), direction-selective cells are abundant and found in most layers. Livingstone thus suggested her model might explain directional selectivity more gen-

erally³, because of widespread asymmetries in dendritic arbors. Here we directly tested Livingstone's hypothesis experimentally in the cat by recording from directional neurons and examining tangential asymmetries in their dendritic trees. We also reconstructed cat and monkey Meynert cells in three dimensions to define their extents and simulated Livingstone's model of dendritic summation in cat and monkey Meynert cells.

RESULTS Experiments

We recorded from 32 single neurons in the cat visual cortex and filled them with horseradish peroxidase (HRP) after mapping their receptive fields. Fixed sections of the brain were processed¹¹ to reveal the neuronal morphology and then osmicated and embedded in resin to eliminate the differential shrinkage of sections prepared for conventional light microscopy. The neurons were then reconstructed in three dimensions by means of a computer-assisted microscope (in-house TRAKA system). The reconstructions were then rotated to the tangential view and projected onto the two-dimensional surface of the visual field representation on the cortex of V1 to determine the relation between their dendrites and direction preferences of their receptive fields. We calculated the dendritic bias (Fig. 1) for the 32 neurons and compared it with their direction preference (Figs. 2 and 3). We reconstructed an additional three Meynert cells from cat (mk) and monkey (mm) for which no physiological data were obtained.

According to Livingstone's hypothesis, the optimum difference between direction of dendritic bias and the preferred direction of motion should be 180° . The observed angular difference between the RF direction preference and the bias angle of the dendritic tree (expressed as the angle, Φ_{max} , of the dendritic tree segment where the summed length of the distal 1/3 of dendrites is greatest, see Fig. 1) is presented in a scatter plot (Fig. 3a). The angular differences cover virtually the entire range, as is emphasized in the frequency plots (Fig. 3b). The distribution of this difference is random

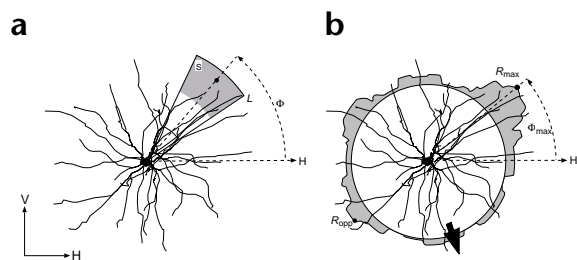


Fig. 1. Computing the dendritic bias. The basal dendrites of a layer 6 pyramidal cell are drawn in a top view; the soma is the blob at the center of the field. **(a)** The distribution of dendritic bias was calculated as follows. The length, L is the Euclidian distance in the two-dimensional projection from the soma to the most distal dendritic tip. Φ is the angle between the midline of the section (dashed line) and the horizontal axis, H . For a given Φ , the summed length (R) of all dendrites lying within the outer third (S) of a 30° segment (shaded area) was calculated. This threshold excluded possible bias from many short dendrites. **(b)** The distribution of R (shaded for visibility), calculated at 1° intervals for the full 360° , is rescaled by $L/(3R_{\max})$ and plotted on a circle of radius $(2/3)L$. R_{\max} is the maximal value obtained for R , R_{opp} indicates the value in the segment directly opposite. Φ_{\max} is the angle of the R_{\max} segment and defines the dendritic bias angle. The receptive field direction preference of the neuron is indicated by the large filled arrow. The directions in the visual field map on the cortical surface are indicated by H (horizontal) and V (vertical). Length of H and V axes is $50 \mu\text{m}$.

(Kolmogoroff-Smirnoff, $p = 0.23$). Increases or decreases in the bin sizes for the segments did not alter this conclusion. Biases derived from the summed dendritic lengths of the total segment or from the inner or middle thirds also gave random distributions.

The asymmetry of the dendritic tree is expressed as the difference (Fig. 3c, ordinate) in the summed length of distal dendrites of opposite segments. If the dendritic tree is exactly symmetrical, then the difference between any pair of opposite segments will be zero. Actually, all neurons showed some degree of asymmetry for some segments of their dendritic tree on this measure. The range of absolute summed dendritic lengths in sector S for opposite segments is indicated by vertical lines (Fig. 3c), along with the difference at Φ_{\max} (filled dot) and the difference at the preferred direction of motion (open squares). These latter differences (open squares) cluster around zero, indicating that there was no dendritic bias along the axis of the preferred direction of motion. Two exceptions show a large negative value, indicating that the longest dendrites are oriented 180° from the preferred direction of motion, as Livingstone's hypothesis

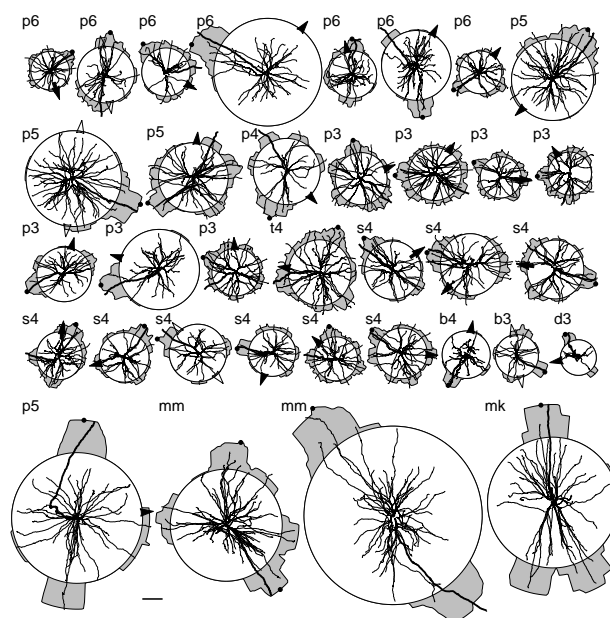
Fig. 2. Directionality and dendritic asymmetry. The basal dendrites of 35 reconstructed cortical neurons are shown as seen from the cortical surface. Shaded area indicates dendritic bias as defined in Fig. 1, plotted on circle of radius $(2/3)L$ (see Fig. 1a). The dendritic path from soma to most distal tip is drawn in bold. Filled dot indicates the angle (Φ_{\max} ; see Fig. 1b) of the segment where dendritic bias was maximal. Arrows and arrowheads indicate angle of preferred direction(s) of motion: filled arrow indicates 'direction selective'; filled arrowhead indicates 'direction preferential'; open arrowheads indicate 'non-directional'. The two monkey Meynert cells (mm) and the cat Meynert cells (mk) were not recorded physiologically. Pyramidal cells in layers 3–6, p3–p6; star pyramidal cells in layer 4, t4; spiny stellate cells in layer 4, s4; basket cells in layers 3 and 4, 3b and 4b; double bouquet cell in layer 3, d3. Simulation results are illustrated for the larger monkey Meynert cell. Scale bar, $100 \mu\text{m}$.

requires. However, such values could occur by chance. The polar plot of the relationship between dendritic bias and directionality (Fig. 3d), in which distance along the radius represents the degree of dendritic asymmetry and the angle represents the difference between Φ_{\max} and the preferred direction of motion, shows that most neurons do not have strong asymmetries, and that few have asymmetries aligned along the appropriate axis.

Simulations

The data presented above exclude the dendrites of cat neurons as the source of structural asymmetry that might produce direction selectivity. Livingstone's generalization to all directional neurons does not hold. Nevertheless, the Meynert cells may be a special case. Because of their scarcity, however, we could not hope to record intracellularly with any frequency from Meynert cells. Thus, we used a detailed compartmental model of the Meynert cells (Fig. 4) to see whether Livingstone's hypothesis might apply in the special case of Meynert cells. Meynert dendrite length (up to $770 \mu\text{m}$) affords the most favorable structure for achieving the asymmetry in temporal summation of synaptic potentials simulated in a previous model⁴.

To simulate the most asymmetrical case possible, we assumed that all retinotopic input was distributed only over the longest basal dendrite of the Meynert cell. Two thousand 'AMPA' excitatory synapses were placed uniformly (1 synapse per $1.5 \mu\text{m}$ of dendritic length) over this dendrite (marked by heavy lines to the right of the soma in Fig. 4a). These excitatory synapses were activated in a temporal sequence, sweeping either from the distal tips towards the proximal dendrites and soma (D–P direction) or in the reverse direction, from the soma towards the distal tips (P–D). We varied the time interval over which the synapses were sequentially activated (the 'sweep duration') and measured the resultant transient voltage response at the soma. The sweep duration simulated the velocity of the stimulus motion across the receptive field of the neuron. Livingstone recorded mainly from neurons with receptive fields at 10 – 15° from the foveal representation. At this eccentricity, 1° of visual space is represented by 1 mm on the cortical surface¹², so a stimulus velocity of 100° per second will give a sweep duration of 10 ms along a 1 mm dendrite. 'GABA_A' inhibitory synapses were placed directly on the model soma and



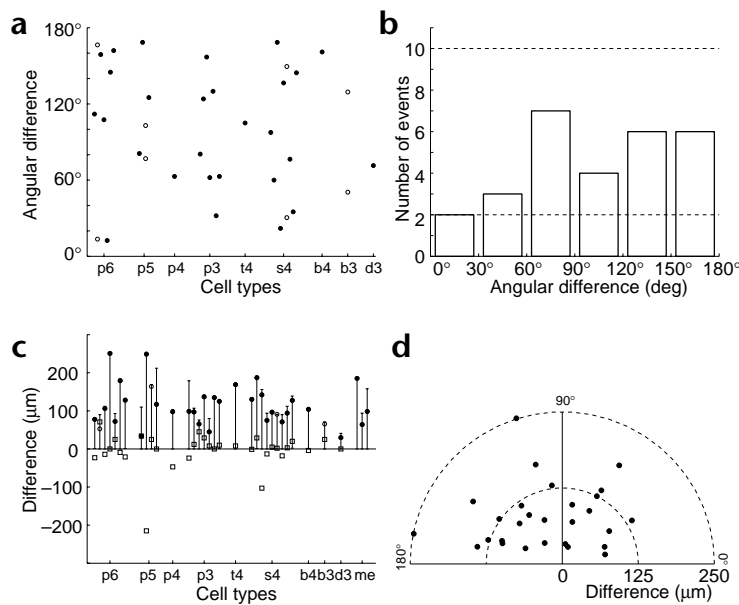


Fig. 3. Analysis of the relationship between directionality and dendritic bias. (a) Filled dots show angular difference between the dendritic bias angle (Φ_{max} ; see Fig. 1b) and the preferred direction of motion. Open dots indicate difference for both directions of motion in nondirectional cells. (b) Histogram of the angular differences (bin size, 30°) shown in (a). Values larger than 10 or smaller than 2 (dashed horizontal lines) are highly unlikely when uniform random distribution is assumed ($p = 0.045$). (c) The asymmetry of the dendritic tree is expressed simply as the difference (ordinate) in the value of R (see Fig. 1) for opposite segments. The range of absolute values of this difference is indicated for each cell by the length of the vertical line, and the actual value at Φ_{max} is indicated for directional cells (filled dots) or nondirectional cells (open dots). Open squares indicate the difference at the angle of the preferred direction of motion. (abbreviations for cell types as in Fig. 3; me, Meynert cells). (d) Polar plot of the relationship between dendrites and directionality. The distance along the radius represents the degree of asymmetry at Φ_{max} ; the angle represents the difference between Φ_{max} and the preferred direction of motion.

activated with a fixed delay of 2 ms following activation of the excitatory synapse located closest to the soma. At peak conductance, these inhibitory synapses reduced the input resistance of the modeled cell to half its resting value, but the exact strength was not critical for the qualitative results obtained below.

The voltage transient was recorded at the soma for a variety of sweep durations (denoted in ms above each transient, Fig. 4b). Sweep duration of zero corresponds to the simultaneous activation of all (2000) excitatory synapses. As shown previously^{4,13}, the expected voltage peak is maximal when the synapses are activated in the D–P direction at the optimal sweep speed. Here the maximal voltage peak was obtained for a sweep duration of 10 ms in the D–P direction. In this case, the membrane time constant, τ_m , was 5 ms. In the null (P–D) direction, the maximal response was obtained for simultaneous activation, and the response decreased as sweep duration increased. The voltage peak at the soma was calculated as a function of the sweep velocity along the longest dendrite (Fig. 4c, bottom, solid line, D–P direction; dashed-dotted line, P–D direction). The preferred velocity in the D–P direction (peak of a continuous curve) was 77 mm per second. This value was obtained by dividing the length of the longest dendrite (0.77 mm) by 10 ms, the optimal sweep duration. Very similar results were obtained for other Meynert cells

and for the comparably long apical dendrite of a pyramidal cell from layer 5 of the cat (not shown).

Intuitively, the optimal sweep duration in the preferred direction should match the propagation velocity of the EPSP as it travels down the dendrite. In this situation, the temporal summation of voltage at the soma will be maximal. Theoretically^{14,15}, in an infinite cylindrical cable, the peak of a passive signal converges to a velocity of $2\lambda/\tau_m$ (two space constants per one time constant) at some distance from the input site. This is shown for the infinite cylinder (Fig. 4d, dashed line). As an approximation, this also applies to the long basal dendrite of the simulated Meynert cell. Because of its complex electromorphology, branch points in the Meynert dendrite generate large transient changes in conduction velocity (Fig. 4d, continuous line). Nevertheless, the average velocity of $2.8\lambda/\tau_m$ for the Meynert dendrite is surprisingly close to that for the infinite cable. We have also computed the average value for the space constant (λ) in this simulated basal dendrite (assuming R_m of 5,000 $\Omega\text{-cm}^2$ and R_i of 150 $\Omega\text{-cm}$) to be 188 μm . With $\tau_m = 5$ ms, this yields a velocity of 75 mm per second, giving an excellent fit with the optimal sweep speed of 77 mm per second computed in Fig. 4c, bottom trace. This optimal velocity ($= 2\lambda/\tau_m$) inversely depends on $\sqrt{R_m}$ (and, thus, is inversely proportional to $\sqrt{\tau_m}$). Increasing τ_m to 50 ms, for example, will reduce the optimal velocity to about 24 mm per s, very close to what was found in the simulations (Fig. 4c, peak of continuous line at top).

What happens when the retinotopic input is mapped over two opposite dendrites rather than over only one dendrite? This case was examined by adding excitatory synapses (with the same density as above) to the opposite (shorter) dendrite (drawn in bold to left of soma in Fig. 4a). In the D–P direction, the input started from the tip of the first dendrite and swept (via the soma) toward the distal tip of the second dendrite. There were two clear differences from the single-dendrite case. First, in the D–P direction, the additional 600 synapses on the shorter dendrite resulted in an increase in the soma peak response only for fast velocities (dashed line, Fig. 4c). There was no change in the peak voltage response for the slower velocities (continuous line, Fig. 4c). Consequently, the clear peak of the velocity profiles (Fig. 4c) that was obtained for activating a single dendrite essentially disappeared in the two-dendrite case. In the latter case, the dendrites behave as a high-pass filter. A second effect of adding an opposite dendrite is that difference between the D–P and the P–D direction (dotted line in Fig. 4c) decreases. This is expected from the reduction of the degree of asymmetry. Indeed, if the two dendrites were identical (complete symmetry), then directionality would be completely lost.

DISCUSSION

The experimental results indicate that the spatial morphological bias of the basal dendrites cannot account for the directionality in the receptive field. Although all dendritic trees contain some asymmetries, there was no correlation of these asymmetries with the preferred direction of motion. Thus, an asymmetric dendritic tree is not in itself a sufficient condition for the generation of a directional receptive field. A corollary of our present findings is that, because direction preference is always orthogonal to the orientation preference, there is also no correlation of dendritic asymmetry with the orientation preference of the receptive field. This

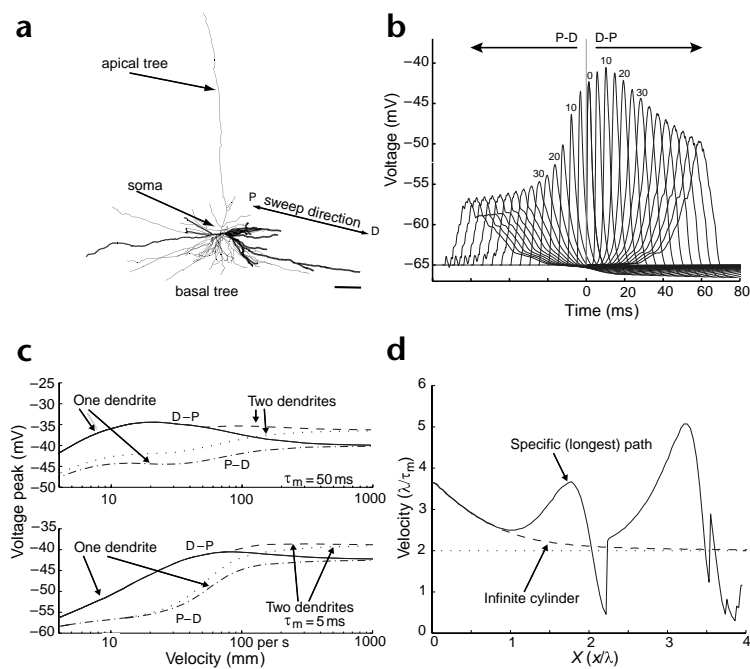


Fig. 4. Modeling directional selectivity of Meynert neuron. **(a)** Meynert cell used for simulation. D, distal; P, proximal. Basal dendrites receiving retinotopic synaptic inputs are drawn in bold. Scale bar, 100 μm . **(b)** Voltage responses at the soma for activation of synaptic inputs in the bold dendrite to the right of the soma in **(a)**. The sweep duration in ms is indicated above the transients. For clarity, each transient in the P-D sweep direction was shifted to the left of the zero time axis by the corresponding sweep duration. **(c)** Peak voltage measured at the soma as a function of the sweep velocity. 'One dendrite' indicates that the retinotopic input was mapped onto the right dendrite drawn in bold in **(a)**; in the 'two dendrites' case, the retinotopic input was distributed over the two opposite dendrites drawn in bold in **(a)**. The top graphs are for $\tau_m = 50$ ms, and the lower graphs are for $\tau_m = 5$ ms. **(d)** Conduction velocity of the peak of a passive EPSP along the path of the longest basal dendrite. Brief α -shaped current input was given at the distal tip of the dendrite ($x = 0$); the soma is at the right end of the x -axis. The conduction velocity of the EPSP peak in an infinitely long passive cylinder is shown by the dashed line. Parameters, $\tau_m = 5$ ms; $R_i = 150 \Omega \cdot \text{cm}$.

result is essentially the same as that obtained previously on a completely different set of neurons in cat visual cortex¹⁶.

The simulations indicated that direction selectivity can, in principle, be computed along individual dendrites of any neuron, given the narrow assumption that the excitatory inputs are mapped in a precise retinotopy along a single dendrite, and no other dendrites are involved. However, even in this tightly constrained case, the major difficulty with this model is that it requires high velocities to work. This is because the optimal sweep speed is directly correlated with the propagation speed of passive signals in dendrites, and because the dendrites are short relative to the magnification factor of the cortical retinotopic map (see above). Here it is important to note that the propagation speed approximates $2\lambda/\tau_m$ (Fig. 4d) and is largely independent of the physical length of the dendrite. The important parameters are the diameter and the specific properties of the membrane and the cytoplasm. Thus, a long, thick apical dendrite and a short, thin basal dendrite can have equivalent velocity characteristics. Our conclusions regarding the asymmetries of the dendritic trees were unaffected, however, even when we converted the morphological dimensions into electrotonic dimensions (not shown). For realistic values of τ_m (~5 millise-

conds in the *in vivo* condition) and for realistic values of λ (a few hundred micrometers), directionality is only achieved when the sweep velocity is very fast (corresponding to stimulus movements of 50–100° per second for 1° per mm magnification).

These theoretical values differ considerably from the velocity tuning of area 17 neurons¹⁷, where the majority of neurons have velocity tuning curves that are low pass in form and have upper cut-off velocities of ~20° per second. In the monkey, Livingstone³ found optimal velocities of 10° per second at eccentricities of 10–15°. At this eccentricity, about 1° of visual field is represented on 1 mm of area 17 (ref. 12), which is similar to the magnification factor for the cat area centralis representation where we recorded. Of course, with active (or synaptic) conductances with slow kinetics, the effective membrane time constant may be slower than the passive value, thus increasing the time window for temporal synaptic integration. The possible influence of these factors is captured in the model by changing τ_m . If τ_m is increased from 5 ms to 50 ms, the membrane depolarizes relatively more for all velocities, and the peak velocity tuning shifts to lower values (Fig. 4c, compare top to bottom). Similarly, the use of delay lines to achieve directionality (for instance, by lagged and nonlagged thalamic relay cells¹⁸) is captured in the model by 'sweeping' the dendrite at different speeds. The effectiveness of the delay lines strongly depends on the membrane time constants and/or the kinetics of the synaptic currents and active membrane conductances (Fig. 4c).

When the retinotopic input is mapped over only one dendrite, the (relative) difference between the preferred and the null direction is maximal. The tuning becomes less sharp when the input is mapped on dendrites that lie opposite each other on both sides of the soma (Fig. 4c, continuous line followed by the dashed line). The velocity profile then tends to be that of a high-pass filter without a distinct peak. In this situation, the difference in voltage response between the preferred and the null direction decreases, and directionality is lost in a completely symmetrical dendritic tree. This implies directionality cannot be achieved by the small dendritic asymmetries that exist in most cat neurons.

The actual time course of the inhibitory synaptic conductance change as derived experimentally in cortical neurons is on the order of 10 ms¹⁹, and this was the value used in our simulations. This is the same order of magnitude as the optimum sweep speed in the cases considered here. Thus, the effect of the inhibition (2 ms delayed) was to abolish most of the response in the null direction. In contrast, in the preferred direction, the peak response was not affected by the inhibition because the voltage peak at the soma preceded the inhibitory input.

Because of ongoing synaptic activity, the membrane potential *in vivo* lies closer to threshold for spike firing than in the passive case studied here, and hence many cortical neurons are spontaneously active. The response of the neuron to stimulus motion thus may result in a change in the firing frequency of the neuron rather than in the occurrence of a spike. The firing frequency is determined by the current or charge generated by the synaptic input (rather than the peak voltage). Unlike the voltage response, the smallest values of the summed synaptic charge seen at the soma are found for fast velocities because the simultaneous activation

of many synapses increases the membrane conductance, and so much more charge is lost via the membrane. As the velocity decreases, less charge is lost through the membrane (not shown). However we found only small differences in the charge entry for the two sweep directions, indicating that directionality is weak when charge is used as the independent variable. An increase in τ_m allows more of the injected charge to reach the soma, but at the cost of reducing the difference between the two sweep directions even further (not shown).

It thus seems fair to conclude that the temporal activation of the dendritic tree by feedforward retinotopic arrays at best might add only a small component to the computation of direction of motion in the visual cortex. Most of the computation of direction of motion over the range of velocities observed must therefore rely on network mechanisms, most probably using the local recurrent circuits of cortex^{20–23}.

METHODS

Preparation of animals and tissue. The neurons examined in this study were obtained from anesthetized adult cats and monkey that had been prepared for *in vivo* intracellular recording (see refs. 24, 25 for details). All experiments were carried out under the authorization of animal research licenses granted by the Home Office of the U.K. and the Cantonal Veterinary Authority of Zürich. In cats, we first recorded from each neuron extracellularly and mapped the receptive field orientation preference, size, type, binocularity and direction preference by hand. Based on strength of directionality, we categorized the neurons in three groups, ‘non-directional’ (when the responses to forward and backward motion were similar), ‘direction preference’ (when responses were clearly biased for one direction of motion) or ‘direction selective’ (where the cell responded almost exclusively to one direction of motion). We compared our qualitative measure with a quantitative direction index, $DI = (\text{preferred} - \text{nonpreferred}) / (\text{preferred} + \text{nonpreferred})$, determined from poststimulus time histograms (PSTHs) made for 23 additional cells recorded in these experiments. Virtually all the cells we classified as directional by hand plotting had DIs in the range 0.5–1.0. This range corresponds to Livingstone’s criterion³ for direction selectivity; that is, “the response to one direction of stimulus motion was at least 3 times larger than the response to the other direction”. The mapping was repeated intracellularly and horseradish peroxidase (HRP) was then ionophoresed into the cell. Under surgical anesthesia, monkey Meynert cells used in the simulations were retrogradely filled from tiny extracellular ionophoretic injections of biocytin into individual layers of area 17. This method fills some neurons in a Golgi-like way. After appropriate survival times, the brains were fixed and processed (by V. Meskenaite) to reveal the biocytin and osmicated and embedded in resin to eliminate differential shrinkage.

Analysis of the dendritic field. To determine the direction bias of the dendritic field, the projection of the dendrites onto the x - z plane (surface view) were used. We have previously established¹⁶ that the vertical meridian of the visual field representation in cat area 17 lies on average at 14° to the parasagittal plane of the stereotaxic coordinate system used for the reconstructions. Extensive mapping was not possible here, but the progression of the receptive fields between successive penetrations was consistent with this general orientation of the retinotopic map. Thus, the surface view of each neuron was rotated 14° to be congruent to the average retinotopic map. Only the basal dendrites of pyramidal cells were considered.

Model neuron. The simulator NEURON²⁶ was used for performing the numerical (compartmental) simulations. The neuron model of the entire dendritic tree was spatially discretized such that each compartment was not larger than 0.1 λ . For R_m of $5 \times 10^3 \Omega\text{-cm}^2$, this gives about 10^3 compartments for the 3 Meynert cells examined. This number was reduced by a factor of about 3 when $R_m = 5 \times 10^4 \Omega\text{-cm}^2$. We examined the performance of the model using two membrane time constants. Because we used $C_m = 1 \mu\text{F per cm}^2$, then $R_m = 5 \times 10^3 \Omega\text{-cm}^2$ implies $\tau_m = 5 \text{ ms}$, and $R_m = 5 \times 10^4 \Omega\text{-cm}^2$ implies $\tau_m = 50 \text{ ms}$. The AMPA-like excitatory synaptic input (modeled as a transient conductance change in the form of an α -

function with maximal conductance, g_{peak} , of 0.4 nS and a time to peak, t_{peak} , of 0.3 ms, in series with a battery of 0 mV) was distributed over the simulated tree at a density of one synapse per 1.5 μm of dendritic length. The inhibitory (GABA_A-like) synaptic input was placed at the model soma and was simulated as a sum of three exponentials; the rising phase was governed by a fast time constant ($\tau_1 = 0.5 \text{ ms}$) and the decay phase by $\tau_2 = 7.5 \text{ ms}$ and $\tau_3 = 33 \text{ ms}$ (see details in ref. 19, Table I). This input was associated with a battery of -70 mV ; it was activated at a fixed delay of 2 ms following the activation of the most proximal excitatory synapse. The peak conductance of all inhibitory synapses was adjusted to equal the input conductance of the modeled cell. Axial resistivity was 150- $\Omega \text{ cm}$.

ACKNOWLEDGEMENTS

This work was supported by an SNF SPP grant to K.A.C.M. and R.J. Douglas and grants to I.S. from the Israeli Academy of Science and the Office of Naval Research. We thank R.J.D. for contributions to the experiments and cell reconstructions.

RECEIVED 18 JUNE; ACCEPTED 15 JULY 1999

- Hassenstein, B. & Reichardt, W. E. in *Proc. 1st Int. Congress Cybernetics Namar* 797–801 (1956).
- Barlow, H. B. & Levick, W. R. The mechanism of directionally selective units in rabbit’s retina. *J. Physiol. (Lond.)* 178, 477–504 (1965).
- Livingstone, M. S. Mechanisms of direction selectivity in macaque V1. *Neuron* 20, 509–526 (1998).
- Rall, W. in *Neural Theory and Modeling* (ed. Reiss, R.) 73–97 (Stanford Univ. Press, Stanford, California, 1964).
- Agmon-Snir, H. & Segev, I. Signal delay and propagation velocity in passive dendritic trees. *J. Neurophysiol.* 70, 2066–2085 (1993).
- Ramon y Cajal, S. Estudios sobre la corteza cerebral humana. *Corteza visual. Revista Trimestral Icorgraphia* 4, 1–63 (1899).
- Le Gros Clark, W. E. The cells of Meynert in the visual cortex of the monkey. *J. Anat.* 76, 369–377 (1942).
- Chan-Palay, V., Palay, S. L. & Billings-Gagliardi, S. M. Meynert cells in the primate visual cortex. *J. Neurocytol.* 3, 631–658 (1974).
- Winfield, D. A., Neal, J. W. & Powell, T. P. S. The basal dendrites of Meynert cells in the striate cortex of the monkey. *Proc. R. Soc. Lond. B Biol. Sci.* 217, 27–40 (1983).
- Winfield, D. A., Rivera-Dominguez, M. & Powell, T. P. S. The number and distribution of Meynert cells in area 17 of the macaque monkey. *Proc. R. Soc. Lond. B Biol. Sci.* 213, 27–40 (1981).
- Adams, J. C. Heavy metal intensification of DAB-based HRP reaction product. *J. Histochem. Cytochem.* 29, 775 (1981).
- Daniel, P. M. & Whitteridge, D. The representation of the visual field on the cerebral cortex in monkeys. *J. Physiol. (Lond.)* 159, 203–221 (1961).
- Segev, I. & Rall, W. Excitable dendrites and spines: Earlier theoretical insights elucidates recent direct observations. *Trends Neurosci.* 21, 453–459 (1998).
- Cole, K. S. C. *Membranes, Ions and Impulses* (Univ. California Press, Berkeley, 1968).
- Jack, J. J. B., Noble, D. & Tsien, R. W. *Electric Current Flow In Excitable Cells* (Clarendon, Oxford, 1975).
- Martin, K. A. C. & Whitteridge, D. The relationship of receptive field properties to the dendritic shape of neurones in the cat striate cortex. *J. Physiol. (Lond.)* 356, 291–302 (1984).
- Orban G. A., Kennedy, H. & Maes, H. Response to movement of neurons in areas 17 and 18 in the cat: direction selectivity. *J. Neurophysiol.* 45, 1043–1073 (1981).
- Saul, A. B. & Humphrey, A. L. Temporal-frequency tuning of direction selectivity in cat visual cortex. *Vis. Neurosci.* 8, 365–372 (1992).
- Galarreta, M. & Hestrin, S. Properties of GABA_A receptors underlying inhibitory synaptic currents in neocortical pyramidal neurons. *J. Neurosci.* 17, 7220–7227 (1997).
- Douglas, R. J. & Martin, K. A. C. A functional microcircuit for cat visual cortex. *J. Physiol. (Lond.)* 440, 735–769 (1991).
- Douglas, R. J., Koch, C., Mahowald, M., Martin, K. A. C. & Suarez, H. H. Recurrent excitation in neocortical circuits. *Science* 269, 981–985 (1995).
- Suarez, H. H., Koch, C. & Douglas, R. J. Modeling direction selectivity of simple cells in striate visual cortex within the framework of the canonical microcircuit. *J. Neurosci.* 15, 6700–6719 (1995).
- Maex, R. & Orban, G. A. Model circuit of spiking neurons generating directional selectivity in simple cells. *J. Neurophysiol.* 75, 1515–1545 (1996).
- Martin, K. A. C. & Whitteridge, D. Form, function and intracortical projections of spiny neurons in the striate visual cortex of the cat. *J. Physiol. (Lond.)* 353, 463–504 (1984).
- Douglas R. J., Martin, K. A. C. & Whitteridge, D. An intracellular analysis of the visual responses of neurones in cat visual cortex. *J. Physiol. (Lond.)* 440, 659–696 (1991).
- Hines, M. L. & Carnevale, N. T. The NEURON simulation environment. *Neural Comput.* 9, 1179–1209 (1997).